

PALS: Distributed Gradient Clocking on Chip

Johannes Bund, Matthias Függer, Moti Medina

Abstract—Consider an arbitrary network of communicating modules on a chip, each requiring a local signal telling it when to execute a computational step. There are three common solutions to generating such a local clock signal: (i) by deriving it from a single, central clock source, (ii) by local, free-running oscillators, or (iii) by handshaking between neighboring modules. Conceptually, each of these solutions is the result of a perceived dichotomy in which (sub)systems are either clocked or asynchronous. We present a solution and its implementation that lies between these extremes. Based on a distributed gradient clock synchronization algorithm, we show a novel design providing modules with local clocks, the frequency bounds of which are almost as good as those of free-running oscillators, yet neighboring modules are guaranteed to have a phase offset substantially smaller than one clock cycle. Concretely, parameters obtained from a 15 nm ASIC simulation running at 2 GHz yield mathematical worst-case bounds of 20 ps on the phase offset for a 32×32 node grid network.

Index Terms—on-chip distributed clock generation, gradient clock synchronization, GALS

1 INTRODUCTION

Consider a circuit of dimension $W \times W$ consisting of comparably small modules of normalized dimension 1 that predominately communicate with physically close modules.

Local clock signals. Each circuit module requires a local clock signal to trigger its computational steps. There are two extreme approaches to provide these clock signals: (i) In the synchronous approach, a clock signal is distributed via a clock tree. The clock’s period is chosen to ensure lock-step computational rounds between all modules and, thus, in particular, for communicating modules. (ii) In the asynchronous approach, modules, potentially as small as a single gate, generate the clock signal locally via handshaking with all communication partners.

From the modules’ perspective, both methodologies provide local clock ticks with different guarantees. We focus on three measures: (a) Whether they ensure a *round structure*, i.e., there is a time-independent tick offset R , such that data that is provided at tick k is guaranteed to be available at the receiving module at tick $k + R$. (b) The *local skew*, i.e., the maximum difference in time between any two k^{th} ticks at modules that communicate with each other. (c) The *waiting time*, i.e., the maximal time between two successive ticks. Note that (b+c) combined with a minimal time between successive ticks allows one to construct a round structure.

Limits of the extremes. Ideally, one would wish for a circuit with a round structure, a small local skew, and a small waiting time. While fully synchronous and asynchronous circuits provide a round structure, they have significant local skew or waiting times. The *local skew* in synchronous

circuits has been shown to *grow linearly* with the circuit width W ; see Section 6.3. On the other hand, causal a-knowledge chains in asynchronous systems can span the entire system, resulting in *waiting times* that *grow linearly* with W .

Fully synchronous or asynchronous systems are indeed rare in practice: in current synchronous systems, there are numerous clock domains with asynchronous interfaces in between [2]. Full asynchronous, delay-insensitive circuits [3] suffer from substantial computational limitations [4], [5], [6] and provide no timing guarantees, rendering them unsuitable for many applications. Accordingly, most real-world asynchronous systems will utilize timing assumptions on some components.

A systematic tradeoff: GALS. Globally Asynchronous Locally Synchronous (GALS) systems [7], [8] are a systematic approach between both extremes. Unlike a single synchronous region (clocked circuits), and no clocked regions (delay-insensitive), GALS systems have several clock islands communicating asynchronously via handshakes. If the width W of the synchronous islands is small, the clock islands can maintain small skew locally. However, the gain comes at the expense of *no round structure*: Clocks on different islands may drift apart arbitrarily. Furthermore, communication across clock domains requires passing through synchronizers [8], [9]. Besides the disadvantage of a *non-zero probability to cause metastable upsets*, the synchronizers incur 2 or more clock cycles of additional *communication latency* if they are in the data path.

Alternative solutions without synchronizers in the data path have been proposed in [10], [11]. The designs either skip clock cycles or switch to a clock signal shifted by half a period when the transmitter and receiver clock risk violating setup/hold conditions. The signal that indicates this choice (skip/switch) is synchronized without additional latency to the data path. Depending on the implementation and intended guarantees, the additional latency is in the order of a clock period. While this can, in principle, be brought down

- J. Bund was with the Engineering Faculty at Bar-Ilan University, Ramat Gan, Israel. Major parts where carried out when J. Bund was with CISA Helmholtz Center for Information Security, Saarland, Germany. E-mail: bundjoh@biu.ac.il
- M. Függer was with CNRS, LMF, ENS Paris-Saclay, Université Paris-Saclay, 91190 Gif-sur-Yvette, France. E-mail: mfuegger@lmf.cnrs.fr
- M. Medina was with the Engineering Faculty at Bar-Ilan University, Ramat Gan, Israel. E-mail: moti.medina@biu.ac.il

A conference version of this work appeared at IEEE ASYNC [1].

to the order of setup/hold-windows, such designs would require considerable logical overhead and fine-tuning of delays. An application-level transmission may be delayed by such a time slot. In [10], this additional delay can be up to 2 clock periods when a so-called no-data packet is oversampled. Further, there is a *non-zero probability of metastable upsets*, and applying such a scheme has to insert no-data packets periodically.

Finally, consider a potential application that runs on top of such schemes and uses handshaking to make sure all its packets of a (logical) time step have arrived before the next time step is locally initiated. It faces the same problem as a fully asynchronous design: the *waiting time grows linearly* with the circuit dimension.

Solutions with round structure. A fully synchronous system provides two convenient properties: (i) metastability-free communication, and (ii) a round structure, that is, no need for handshaking between the synchronous islands of a GALS system. Abandoning the synchronous structure leads to the loss of these properties.

Solutions that directly provide a round structure have been proposed. Examples are GALS architectures with pausable clocks [12], [13], distributed clock generation algorithms like DARTS [14] and FATAL [15], wave clock distribution [16], and distributed clocking grids [17]. However, pausable clocks suffer from potentially unbounded waiting times due to metastability, and DARTS and FATAL require essentially fully connected communication networks. The solution in [16] employs analog cross-coupling of clock buffers to distribute a single clock source over a grid network. Here, we show how to design a purely digital system that utilizes an algorithmic approach to synchronize many clock domains. A digital version of the Fairbanks clock generation grid [17] is analyzed in this work and shown to lead to linear waiting times; see Section 6.4.

The PALS approach. In this work, we present a different approach that combines a *round structure* with *low local skew*, a *low waiting time*, and *provable absence of metastable-upsets*. The PALS approach can be regarded as a drop-in replacement for GALS systems; it uses locally synchronous islands and global communication between islands. It improves over GALS systems by adding a round structure.

Our design is based on the *distributed gradient clock synchronization (GCS) algorithm* by Lenzen et al. [18], in which the goal is to minimize the worst-case clock skew between adjacent nodes in a network. In our setting, the modules correspond to nodes; an edge connects them if they directly communicate (i.e., exchange data). More precisely, let D be the diameter of the network and ρ be the (unintended) drift of the clock of a clocked region, $\mu > 2\rho$ a freely chosen constant, and δ an upper bound on how precisely the phase difference to neighboring clocked regions is known. Then:

- The synchronized clocks are guaranteed to run at normalized rates between 1 and $(1 + \mu)(1 + \rho)$, i.e., have *constant waiting time*.
- The *local skew* is bounded by $\mathcal{O}(\delta \log_{\mu/\rho} D)$.
- The *global skew*, i.e., the maximum phase offset between any two nodes in the system, is $\mathcal{O}(\delta D)$.

In other words, the synchronized clocks are almost as good as free-running clocks in a GALS system, with drift ρ , yet the *local skew* grows only *logarithmically in the chip width W* .

We extend the conference version [1] by an in-depth analysis of the PALS algorithm and additional simulations demonstrating its performance. We further add a comparison to a state-of-the-art clock generation grid [17].

Outline and results. After the introduction in this section, we discuss the computational model in Section 2. In Section 3, we briefly present the GCS algorithm before discussing a variant of the algorithm (called *OffsetGCS*) used in this work. We break down the *OffsetGCS* into hardware modules and specify these modules in Section 4. The algorithm carried out by the hardware modules is denoted by *ClockedGCS*. Our main theorem (Theorem 4.6) states that every hardware system that implements *ClockedGCS* maintains the skew bounds of the GCS algorithm. An implementation of the hardware modules on register-transfer-level, which we denote by *GCSoC*, is discussed in Section 5. We conclude this work with simulations of this implementation in Section 6. Implementation and simulation are carried out in the 15 nm FinFET-based NanGate OCL [19]. For 2 GHz clock sources with an assumed drift of $\rho = 10^{-5}$, and $\mu = 10^{-3}$, our simple sample implementation guarantees that $\delta \leq 5$ ps in the worst case. The resulting local skew is 20 ps, which is well below a clock cycle. We stress that this enables much faster communication than handshake-based solutions, which incur synchronizer delay. We conclude with a comparison of the performance of our solution by SPICE simulations to a digital version of a Fairbanks grid.

2 COMPUTATIONAL MODEL

Network, Communication, and Timing. The network of communicating synchronous PALS islands is modeled by an undirected graph $G = (V, E)$, where the set of nodes V is the set of islands and there is an edge $(v, w) \in E$, if v and w communicate. Edges are bidirectional, i.e., edges (v, w) and (w, v) are the same edge. Furthermore, for each $v \in V$, E contains edge (v, v) . The diameter D of a network is the maximum distance over all pairs of nodes, where the distance between two nodes is the length of a shortest path connecting those nodes in the network.

We denote real time, i.e., an external reference time for analysis, by *Newtonian* time. A node has no access to Newtonian time, but has its own (internal) time reference.

Nodes communicate by sending content-less messages, known as *pulses*. A pulse is sent via broadcast to all neighboring nodes. The message delay is the time a pulse travels between the sender and receiver. It is constrained by a maximum delay d and a minimum delay $d - U$, where U is the delay uncertainty. A pulse sent by a node at Newtonian time t is received between time $t + d - U$ and time $t + d$.

Hardware Clock. Each node can locally measure the progress of time. For example, a node may do this via a local ring oscillator. For the analysis, we abstract any such device by the mathematical concept of a *hardware clock*. A hardware clock is prone to uncertainty, which we model by a variable rate that may change over time. The uncertainty is called the *hardware clock drift* (short *clock drift*). Formally, for each

node $v \in V$ there is an integrable function $h_v: \mathbb{R}_{\geq 0} \rightarrow \mathbb{R}$ called the hardware clock rate. Parameter $\rho > 0$ is an upper bound on the one-sided hardware clock drift of all nodes. The hardware clock rate satisfies $1 \leq h_v(t) \leq 1 + \rho$ for all $t \in \mathbb{R}_{\geq 0}$. The hardware clock value of v at time t , $H_v(t)$, is then defined by

$$H_v(t) = \int_0^t h_v(\tau) d\tau + H_v(0),$$

where $H_v(0)$ is the initial value of v 's hardware clock at Newtonian time 0. A node that has measured its hardware clock to advance by T knows that the real time difference is in $[T/(1 + \rho), T]$.

Logical Clock. While a hardware clock allows a node to measure time differences, its rate cannot be controlled. The logical clock is a hardware clock that can also be controlled. Indeed, we will use an adjustable ring oscillator in this work as a logical clock. Formally, the local clock signal a node produces is given by $L_v: \mathbb{R}_{\geq 0} \rightarrow \mathbb{R}$, where $L_v(t)$ is the phase (normalized by 2π) of the clock signal since the first clock tick.¹ A node's logical clock is initialized to $H_v(0)$ and follows the hardware clock's rate but is adjustable by a constant factor. In our algorithm, the logical clock will be implemented by the node's local adjustable ring oscillator that has only two modes: slow and fast. Their rate differs by factor μ , slow has (normalized) rate 1 and fast has $(1 + \mu)$.

Skew. The skew between two nodes describes the difference in their logical clock values. The upper bound on the skew is a figure of merit for clock synchronization algorithms. We regard two types of skew in a system, the *global skew* and the *local skew*.

Definition 2.1 (global and local skew). *The global skew $\mathcal{G}(t)$ is the maximum skew between any two nodes in the network. Formally, it is defined by*

$$\mathcal{G}(t) := \max_{v, w \in V} \{L_w(t) - L_v(t)\}.$$

The local skew $\mathcal{L}(t)$ is the maximum skew between any two neighboring nodes in the network. Formally, it is defined by

$$\mathcal{L}(t) := \max_{(v, w) \in E} \{L_w(t) - L_v(t)\}.$$

Our Goal. Given a network of nodes and the nodes' local oscillator parameters, the goal is to provide an algorithm (i.e., a circuit) that controls the slow and fast clock speed signals at each node such that small, bounded, local, and global skews are ensured.

3 ALGORITHM AND SKEW BOUND GUARANTEES

3.1 Gradient Clock Synchronization

We start by recalling the class of GCS algorithms studied by Lenzen et al. [18].

Intuitively, a GCS algorithm executed by node v continuously measures the skew to each neighbor w . By a set of rules, the algorithm decides whether to progress the

logical clock at a fast or a slow rate. Lenzen et al. showed that such GCS algorithms achieve close synchronization between neighboring nodes in an arbitrary network, i.e., minimize $\mathcal{L}(t)$. Let δ be an upper bound on how precisely the skew between neighbors is known. Provided that the global skew does not exceed a bound of $\mathcal{O}(\delta D)$, GCS achieves asymptotically optimal local skew bounded by $\mathcal{O}(\delta \log_{\mu/\rho} D)$. In other words, local skew grows only logarithmically in the hop diameter of the network; still, we have clocks that progress at a minimum rate of 1. The local and global skew bounds are asymptotically optimal [18].

3.2 GCS and OffsetGCS Algorithm

The GCS algorithm by Lenzen et al. computes a logical clock from the hardware clock in two different modes, fast and slow. In slow mode, the logical clock follows the rate of the hardware clock. In fast mode, the logical clock advances at the hardware clock rate and *speedup factor* $\mu > 0$. Formally, a node in fast mode advances its logical clock with rate $(1 + \mu)h_v(t)$, where μ is chosen by the designer. A node controls its binary mode signal $\gamma_v(t) \in \{0, 1\}$ to adjust its logical clock. In *fast mode* γ_v is set to 1 and, accordingly, in *slow mode* γ_v is set to 0. The logical clock value of v at time t with initial value $H_v(0)$ thus is

$$L_v(t) = \int_0^t (1 + \mu \cdot \gamma_v(\tau)) h_v(\tau) d\tau + H_v(0).$$

A node in fast mode must be able to catch up to a node in slow mode. Hence, we pose the constraint that fast mode (without clock drift) can never be slower than slow mode (with clock drift). This can be formalized as

$$1 + \rho < 1 + \mu.$$

The algorithm specifies two conditions that control when to switch between fast and slow modes. Accordingly, conditions are named *fast condition* (FC) and *slow condition* (SC). The algorithm is parameterized by κ , which determines the synchronization quality.

Definition 3.1 (fast and slow condition). *Let $\kappa \in \mathbb{R}^+$ be a positive, non-zero, real number. A node $v \in V$ satisfies the fast condition at time t if there is a natural number $s \in \mathbb{N} = \{0, 1, \dots\}$ such that both:*

$$\exists (v, x) \in E : L_x(t) - L_v(t) \geq (2s + 1)\kappa \quad (\text{FC-1})$$

$$\forall (v, y) \in E : L_y(t) - L_v(t) \geq -(2s + 1)\kappa \quad (\text{FC-2})$$

Node $v \in V$ satisfies the slow condition at time t if there is a natural number $s \in \mathbb{N}$ such that the following conditions hold:

$$\exists (v, x) \in E : L_x(t) - L_v(t) \leq -2s\kappa \quad (\text{SC-1})$$

$$\forall (v, y) \in E : L_y(t) - L_v(t) \leq 2s\kappa \quad (\text{SC-2})$$

Node v satisfies the fast condition if there is at least one node u , that is ahead of v and no other node behind v exceeds the absolute skew between v and u . The slow condition is satisfied if there is a node u behind v that has a larger absolute skew to v than all nodes ahead of v . The thresholds use odd multiples of κ for the fast condition and even multiples of κ for the slow condition to ensure mutual exclusion.

1. For example, a (perfect, non-drifting) logical clock with frequency f has phase $2\pi \cdot f \cdot t$ at time t , and normalized (by 2π) phase $f \cdot t$. The logical clock thus advances by a full step of one every $1/f$ time but continuously advances in between.

If v is the node with the largest logical clock value in the network, then all other nodes are behind v , they have negative skew. Thus, the slow condition is satisfied for $s = 0$. Accordingly, if v is the node with the smallest clock value in the network, then it satisfies the fast condition as all skews to other nodes are positive.

Definition 3.2. An algorithm is a GCS algorithm with parameters ρ, μ, κ if the following invariants hold, for every node $v \in V$ and all times t, t' :

$$\mu > \rho \quad (\text{I1})$$

$$L_v(t') - L_v(t) \in [1, 1 + \mu] \cdot (H_v(t') - H_v(t)) \quad (\text{I2})$$

$$\text{if } v \text{ satisfies FC at time } t \text{ then } v \text{ is in fast mode at time } t \quad (\text{I3})$$

$$\text{if } v \text{ satisfies SC at time } t \text{ then } v \text{ is in slow mode at time } t \quad (\text{I4})$$

Invariant (I2) states that the rate of the logical clock is at least the rate of the hardware clock and at most $(1 + \mu)$ times the rate of the hardware clock.

Remark. Every algorithm that meets Definition 3.2 is a GCS algorithm. In this work we focus on the algorithm by Lenzen, Locher, and Wattenhofer [18], which we state in Algorithm 1.

Maximal and Minimal Offsets. The conditions in Definition 3.1 can be reformulated using the maximal and minimal offset. Maximal and minimal offsets at node v are given by

$$O_{\max}(t) := \max_{(v,x) \in E} \{L_x(t) - L_v(t)\}, \quad (\text{3})$$

$$O_{\min}(t) := \min_{(v,x) \in E} \{L_x(t) - L_v(t)\}. \quad (\text{4})$$

The node with the largest offset to v is the node that is ahead of v the most, and the node with the smallest offset to v is the node most behind v .

A node $v \in V$ satisfies the fast condition if some neighbor reached a (positive) threshold and no other neighbor crossed the corresponding negative offset. If the $O_{\max}(t)$ reached a certain threshold we are certain that some neighbor reached this offset. Accordingly if $O_{\min}(t)$ is larger than the corresponding negative offset, no neighbor crossed the corresponding negative offset. Formally, we replace Eqs. (FC-1) and (FC-2) and Eqs. (SC-1) and (SC-2) in Definition 3.1 by

$$O_{\max}(t) \geq (2s + 1)\kappa, \quad (\text{FC-1})$$

$$O_{\min}(t) \geq -(2s + 1)\kappa, \quad (\text{FC-2})$$

$$O_{\min}(t) \leq -2s\kappa, \text{ and} \quad (\text{SC-1})$$

$$O_{\max}(t) \leq 2s\kappa. \quad (\text{SC-2})$$

Offset Estimates. Nodes have no access to logical clocks of their neighbors. Hence, precise skews remain unknown to the node. In order to fulfill the invariants of the algorithm a node maintains an estimate of each offset to a neighbor. Offset and skew are the same, we use the terms interchangeably. The *offset estimate* of node v to its neighbor w is denoted by \widehat{O}_w . Intuitively, we have $\widehat{O}_w(t) \approx L_w(t) - L_v(t)$. Parameter δ gives a two-sided bound on the estimates.

$$\left| \widehat{O}_w(t) - (L_w(t) - L_v(t)) \right| \leq \delta \quad (\text{5})$$

Algorithm 1 GCS algorithm at node v , where $\text{ft}1_s, \text{ft}2_s$, and o_w are variables.

```

1: at each time  $t$  do
2:   for each neighbor  $w$  do
3:      $o_w \leftarrow \widehat{O}_w(t)$  ▷ save offset estimate to  $w$ 
4:    $\text{ft}1_s \leftarrow \exists w : o_w \geq (2s + 1)\kappa - \delta$ 
5:    $\text{ft}2_s \leftarrow \forall w : o_w \geq -(2s + 1)\kappa - \delta$ 
6:   if  $\exists s : \text{ft}1_s \wedge \text{ft}2_s$  then
7:      $\gamma_v(t) \leftarrow 1$  ▷ switch to fast mode
8:   else
9:      $\gamma_v(t) \leftarrow 0$  ▷ switch to slow mode

```

Given an estimate of each neighboring clock, the GCS algorithm specifies the *fast trigger* (FT). Each node determines by FT whether to go fast or slow. A node that satisfies FC must satisfy FT, but a node that satisfies SC must not satisfy FT.

Definition 3.3 (fast trigger). Let $\kappa \in \mathbb{R}^+$ be a positive, non-zero, real number. A node $v \in V$ satisfies the fast trigger at time t if there is a natural number $s \in \mathbb{N}$ such that both:

$$\exists (v, x) \in E : \widehat{O}_x(t) \geq (2s + 1)\kappa - \delta \quad (\text{FT-1})$$

$$\forall (v, y) \in E : \widehat{O}_y(t) \geq -(2s + 1)\kappa - \delta \quad (\text{FT-2})$$

We are now able to state the GCS algorithm in Algorithm 1. Intuitively, the GCS algorithm checks the FT at all times. If v satisfies FT then v switches to fast mode, otherwise v defaults to slow mode.

Remark. As the decision to run fast or slow is a discrete decision, a circuit implementation will be prone to metastability [20]. We focus on this problem in Section 4.4.

Maximal and Minimal Offset Estimates. The fast trigger of Lenzen et al. can be redefined using the largest and smallest offset estimate of node v . We define the maximal and the minimal estimate of v 's offset estimates by

$$\widehat{O}_{\max} := \max_{(v,x) \in E} \{\widehat{O}_x\}, \text{ and } \widehat{O}_{\min} := \min_{(v,x) \in E} \{\widehat{O}_x\}.$$

Then, we replace Eqs. (FT-1) and (FT-2) in Definition 3.3 by

$$\widehat{O}_{\max}(t) \geq (2s + 1)\kappa - \delta, \quad (\text{FT-1})$$

$$\widehat{O}_{\min}(t) \geq -(2s + 1)\kappa - \delta. \quad (\text{FT-2})$$

We are thus able to restate the GCS algorithm (Algorithm 1) in Algorithm 2. Rather than quantifiers “exists” and “for all” over all outgoing edges we make use of \widehat{O}_{\max} and \widehat{O}_{\min} . The algorithm, referred to as *OffsetGCS*, is stated in Algorithm 2.

Next, we show that in *OffsetGCS* we can also bound the number of thresholds, i.e., we bound the maximum value of s in Algorithm 1, line 6.

Bound on s . In case of a bounded local skew, which we will later show to be the case, we can bound the maximal number of steps s that need to be measured. Let $\mathcal{L} := \sup_t \mathcal{L}(t)$ be the largest skew between two neighbors. Let ℓ be the largest number such that $(2\ell + 1)\kappa - \delta \leq \mathcal{L}$. Then, node $v \in V$ satisfies the fast trigger at time t if there is an $s \in [\ell + 1]$ such that Eqs. (FT-1) and (FT-2) hold.

Visualization. In Fig. 1 we depict the conditions of *OffsetGCS*. Along the axis we mark the offsets, where the

Algorithm 2 OffsetGCS algorithm at node v , where o_w , o_{\max} , o_{\min} , $ft1_s$, and $ft2_s$ are variables that store a value.

```

1: at each time  $t$  do
2:   for each adjacent node  $w$  do
3:      $o_w \leftarrow \hat{O}_w(t)$   $\triangleright$  save offset estimate to  $w$ 
4:    $o_{\max} \leftarrow \max_{(v,w) \in E} \{o_w\}$   $\triangleright$  compute and save max
5:    $o_{\min} \leftarrow \min_{(v,w) \in E} \{o_w\}$   $\triangleright$  and min estimates
6:   for  $s \in [\ell + 1]$  do
7:      $ft1_s \leftarrow o_{\max} \geq (2s + 1)\kappa - \delta$ 
8:      $ft2_s \leftarrow o_{\min} \geq -(2s + 1)\kappa - \delta$ 
9:   if  $\exists s \in [\ell + 1] : ft1_s \wedge ft2_s$  then
10:     $\gamma_v(t) \leftarrow 1$   $\triangleright$  switch to fast mode
11:   else
12:     $\gamma_v(t) \leftarrow 0$   $\triangleright$  switch to slow mode

```

x -axis marks the maximal and the y -axis marks the minimal offset. Conditions FC, SC and FT can be marked as areas. The fast condition, defined by Eqs. (FC-1) and (FC-2), is marked in yellow. The slow condition, defined by Eqs. (SC-1) and (SC-2), is marked in blue. The fast trigger, defined by Eqs. (FT-1) and (FT-2), is a translation of FC by δ to the left and δ down. It is marked by the orange are (including the yellow area). We require that $\kappa > 2\delta$ (see Definition 3.5), thus, the gap between FC and SC is larger than 2δ .

Fix a node v , we mark maximal and minimal offsets as a point (O_{\min}, O_{\max}) . In the GCS algorithm v goes to fast mode at any time where (O_{\min}, O_{\max}) falls into the FC (yellow) region. Similarly, if (O_{\min}, O_{\max}) falls into the SC (blue) region, v goes to slow mode. In between both regions v is free to choose any speed between fast and slow mode. The offset estimates of v are given by point $(\hat{O}_{\min}, \hat{O}_{\max})$, which we mark as a cross. Due to Eq. (5) the cross may fall into the δ surrounding of (O_{\min}, O_{\max}) . We mark this by a larger box surrounding (O_{\min}, O_{\max}) .

A node that executes OffsetGCS chooses to go to fast or slow mode depending on whether $(\hat{O}_{\min}, \hat{O}_{\max})$ falls into the FT (orange and yellow) region. From the visualization one can see that for any (O_{\min}, O_{\max}) in the FC region, $(\hat{O}_{\min}, \hat{O}_{\max})$ will be within the FT region, and can never cause OffsetGCS to go slow. Similarly any (O_{\min}, O_{\max}) in the SC region can never cause OffsetGCS to go fast.

3.3 Analysis of the OffsetGCS Algorithm

In what follows, we prove that for a suitable choice of parameters (i.e., ρ , μ , κ , δ , and ℓ), OffsetGCS is a GCS algorithm as defined in Definition 3.2. Theorem 3.4 implies that OffsetGCS maintains tight skew bounds. For the proof of Theorem 3.4, we refer the reader to [21].

Theorem 3.4. *Suppose algorithm A is a GCS algorithm according to Definition 3.2 with $\mu > 2\rho$. Then, A maintains global and local skew of*

$$\mathcal{G}(t) \leq \frac{\mu\kappa D}{\mu - 2\rho} \quad \mathcal{L}(t) \leq \left(\left\lceil \log_{\mu/\rho} \frac{\mu D}{\mu - 2\rho} \right\rceil + 1 \right) \kappa$$

either 1) for all $t > 0$ if $\mathcal{L}(0) \leq \kappa$ or 2) for sufficiently large $t \geq T$, where $T \in \mathcal{O}((\mathcal{G}(0) + \kappa D)/(\mu - 2\rho))$.

Uncertainty sources in OffsetGCS implementations. In our analysis, we distinguish between two sources of un-

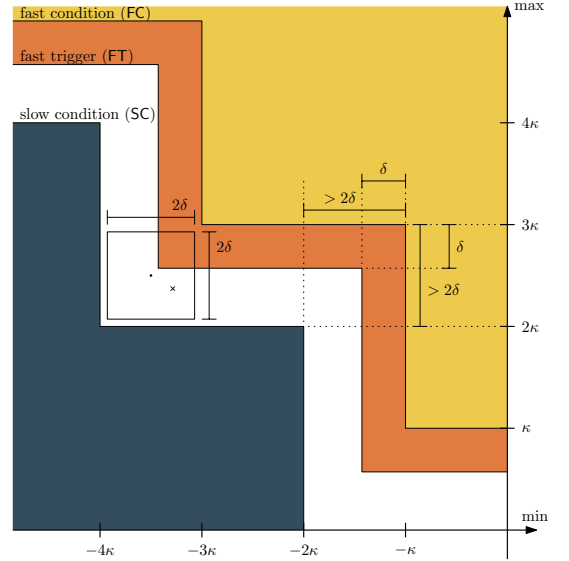


Fig. 1: Visualization of FC, SC and FT in the plane of min and max of the offsets. The exact measurement (O_{\min}, O_{\max}) is denoted by a point. The actual measurement $(\hat{O}_{\min}, \hat{O}_{\max})$ is depicted as a small cross. We denote the maximum measurement error by a square surrounding the exact measurement. The OffsetGCS algorithm switches to fast when $(\hat{O}_{\min}, \hat{O}_{\max})$ is within the FT region and to slow otherwise.

certainty: (i) The *propagation delay uncertainty* δ_0 . This is the absolute timing variation added to the measurement error due to propagation delays, e.g., wire and gate delays on the path from the clock source to the measurement module. (ii) The measurement error resulting from unknown clock rates. Denote by T_{\max} the *time between initiating a measurement and using it to control the logical clock speed*. During this time, logical clocks advance at rates that are not precisely known. This adds to the measurement error because the actual difference might increase or decrease compared to the measured difference.

We denote an upper bound on the combined error by δ ; the relation of δ to δ_0 and T_{\max} is elaborated in Section 4.4. Given δ , we seek to choose κ as small as possible to obtain a small local skew bound according to Theorem 3.4. In the following, we show constraints on parameters like κ such that an instance of OffsetGCS, we will refer to it as a particular implementation of OffsetGCS, is a GCS algorithm.

Theorem 3.5. *An implementation of OffsetGCS is a GCS algorithm if for all times t it satisfies (i) $\mu > 2\rho$ (ii) $|\hat{O}_w(t) - (L_w(t) - L_v(t))| \leq \delta$ (iii) $\kappa > 2\delta$ (iv) $\sup\{s \in \mathbb{N} | (2s + 1)\kappa \leq \mathcal{L} + 2\delta\} \leq \ell < \infty$*

Proof. To show the statement, we verify the conditions of Definition 3.2. By assumption condition (I1) is satisfied. Condition (I2) is a direct consequence of the algorithm specification. For Condition (I3), suppose first that v satisfies the fast condition at time t . There exists some $s \in \mathbb{N}$ and neighbor x of v such that $L_x(t) - L_v(t) \geq (2s + 1)\kappa$. Therefore, by (5), $\hat{O}_x(t) \geq (2s + 1)\kappa - \delta$, so that (FT-1) is satisfied. Further, from the definitions of the local skew

and δ , $\mathcal{L} + \delta \geq \widehat{O}_x(t)$. Combining the above inequalities yields $\mathcal{L} + \delta \geq (2s + 1)\kappa - \delta$. By assumption, s fulfills $s \leq \ell < \infty$. Thus, $\text{ft}1_s$ is set to true.

Similarly, since v satisfies the fast condition, all of its neighbors y satisfy $L_v(t) - L_y(t) \leq (2s + 1)\kappa \leq \mathcal{L}$. Therefore, $\widehat{O}_y(t) \geq -(2s + 1)\kappa - \delta \geq -\mathcal{L} - \delta$, hence (FT-2) is satisfied for the same value of s . From $-(2s + 1)\kappa - \delta \geq -\mathcal{L} - \delta$, it is $(2s + 1)\kappa \leq \mathcal{L}$. Thus, $s \leq \ell < \infty$ and $\text{ft}2_s$ is set to true. Consequently, v runs in fast mode at time t .

It remains to show that if v satisfies SC at time t , it does not satisfy FT at time t and is in slow mode. Suppose, for contradiction, that v satisfies SC and FT at time t . Fix $s \in \mathbb{N}$ such that SC is satisfied and $s' \in \mathbb{N}$ such that FT is satisfied. Then, by (5) and SC-2,

$$\widehat{O}_{\max}(t) \leq 2s\kappa + \delta.$$

Thus, by FT-1, $(2s' + 1)\kappa - \delta \leq 2s\kappa + \delta$. Since $2\delta < \kappa$, the previous expression implies that $s' < s$. Similarly, by (5), SC-1, and FT-2 we obtain $-2s\kappa \geq -(2s' + 1)\kappa - \delta$, such that, $s < s' + 1$. However, this contradicts $s' < s$. Thus FT cannot be satisfied at time t if SC is satisfied at time t , as we assumed. \square

Combining Theorems 3.4 and 3.5, we finally obtain that an implementation of OffsetGCS fulfilling the conditions in Theorems 3.5, maintains the skew bounds in Theorem 3.4.

4 DECOMPOSITION INTO MODULES

To implement the OffsetGCS algorithm in hardware, we break down the distributed algorithm in this section into circuit modules. Here we are concerned with the clock generation network that comprises an arbitrary number of nodes connected by links. To focus on the clock generation circuitry, we do not discuss the circuitry for the data communication infrastructure that can be implemented using gradient clocking and communication links between clocked modules.

We distinguish between the implementation of a node and the implementation of a link.² Per node, we have a *tunable oscillator* that is responsible for maintaining the logical clock of a node, and a *control module* that sets the local clock speed if the fast trigger FT is fulfilled. Per link, we have two *phase offset measurement modules*, one for each node connected by the link, that measures the clock offset $\widehat{O}_w(t)$ of a node to its neighbor w (see Figure 8 for a high-level architecture comprising of the control module, the VCO as the tunable oscillator, and the measurement modules).

Metastability-Containing Implementation. The three modules form a control loop: Skews are measured and fed into the control module, which acts upon the tunable oscillator. Any measurement circuit that round-wise measures a continuous variable, in our case, the skew, and outputs a digital representation can be shown to become metastable [20]. In [24], a technique to compute with such metastable or unstable signals was presented. The term *metastability-containing* circuit was coined for a circuit that guarantees that the provably minimal amount of metastability carries over from

the inputs to the outputs. In this work, we will build on this technique and design the circuitry to be metastability-containing: (i) The measurement circuit outputs the minimal number of metastable outputs, (ii) the controller only produces metastable outputs if its inputs are unstable, and (iii) the tunable oscillator frequency is bounded even in the presence of metastable/unstable signals.

4.1 Tunable Oscillator

The logical clock signal of node v is derived from a tunable oscillator. Each node is associated with its own oscillator that can be tuned in its frequency. The tunable oscillator module has one input and one output port. The binary input md_v controls the mode (slow/fast) of the oscillator. The binary output clk_v is the oscillator's binary clock signal whose phase is the logical clock L_v . The oscillator has a maximum response time $T_{\text{osc}} \geq 0$, by which it is guaranteed to change frequency according to the mode signal. Formally, we require the following conditions to hold:

$$\mathcal{L}(0) < \kappa. \quad (\text{C1})$$

If mode signal of node v is constantly 0 for time T_{osc} , the oscillator with output clk_v is in *slow mode* at time t :

$$\forall t' \in [t - T_{\text{osc}}, t]. \text{md}_v(t') = 0 \Rightarrow L_v(t) \in [1, 1 + \rho]. \quad (\text{C2})$$

If a mode signal is constantly 1 for time T_{osc} , the respective oscillator is in *fast mode* at time t :

$$\begin{aligned} \forall t' \in [t - T_{\text{osc}}, t]. \text{md}_v(t') = 1 \Rightarrow \\ L_v(t) \in [1 + \mu, (1 + \mu)(1 + \rho)]. \end{aligned} \quad (\text{C3})$$

Otherwise, the respective oscillator is *unlocked* at time t :

$$\begin{aligned} \exists t', t'' \in [t - T_{\text{osc}}, t]. \text{md}_v(t') \neq \text{md}_v(t'') \Rightarrow \\ L_v(t) \in [1, (1 + \mu)(1 + \rho)]. \end{aligned} \quad (\text{C4})$$

The requirements on the oscillator are as follows: if the control signal is stable for T_{osc} time, the oscillator needs to guarantee the respective frequency. At any other time, it is not locked to a fixed mode and may run at any frequency between the slowest and fastest possible. In particular, the unlocked mode may be entered when the mode signal is metastable, unstable, or transitioned recently, i.e., an oscillator that satisfies (C4) can cope with meta-/unstable inputs in the sense that it produces stable outputs. We stress that a tunable oscillator satisfying (C4) is not pausable.

It is an essential requirement of the algorithm that the skew between two nodes cannot increase if the algorithm tries to reduce that skew. We maintain the requirement $\mu > 2\rho$, ensuring that the phase offset between the two clocks cannot increase further when a clock in fast v mode is chasing a clock in slow mode.

4.2 Phase Offset Measurement Module

To check whether the FT conditions are met, a node v needs to measure the current phase offset $L_w(t) - L_v(t)$ to each neighbor w . This is achieved by a time offset measurement module between v and each neighbor w . Node v has no direct access to $L_w(t)$ as propagation delays are prone to uncertainty. Hence, a node can only estimate the offset to w , where the offset estimate is denoted by $\widehat{O}_w(t)$.

2. For an in-depth survey of related work and state-of-the-art link-level FIFO buffer controllers, we refer the reader to [22], [23].

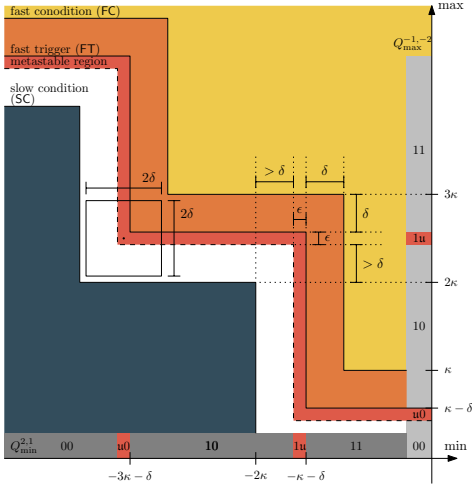


Fig. 2: Update of Fig. 1 including the decision separator. As in Fig. 1 we visualize FC and SC with respect to O_{\min} and O_{\max} . FT and the metastable region are visualized with respect to \hat{O}_{\min} and \hat{O}_{\max} . Along the axis we show the encodings $Q_{\min}^{2,1}$ and $Q_{\max}^{-1,-2}$, marking also the effect of meta-/instability.

Inputs to the offset measurement are signals clk_v and clk_w . The outputs are denoted by $q_w^{\pm i}(t)$ for $i \in \{1, \dots, \ell\}$. They represent a unary encoding of $\hat{O}_w(t)$ of length 2ℓ . As mentioned before, the offset measurement module may produce metastable estimates. We next discuss the module's specifications.

Thresholds. The algorithm does not require full access to the function $\hat{O}_w(t)$, but only to whether $\hat{O}_w(t)$ has reached one of the thresholds defined by (FT-1) and (FT-2). FT defines infinitely many thresholds, i.e., the algorithm has to check for each $s \in \mathbb{N}$ whether (FT-1) or (FT-2) is satisfied.

However, practically the system can only measure finitely many thresholds. Since the algorithm guarantees a maximum local skew, there is a maximum s until which the algorithm needs to check. Let $\ell \in \mathbb{N}$ be the largest number such that $(2\ell + 1)\kappa + \delta < \mathcal{L}$, where \mathcal{L} is the upper bound on the local skew. Then $\hat{O}_w(t)$ is defined as a binary word of length 2ℓ . The bits are denoted (from left to right) by $Q_w^\ell, \dots, Q_w^1, Q_w^{-1}, \dots, Q_w^{-\ell}$. For $i \in \{1, \dots, \ell\}$ each output bit $Q_w^{\pm i}(t)$ denotes whether $\hat{O}_w(t)$ has reached the corresponding threshold. For example, a module with $\ell = 2$ has 4 outputs Q_w^2, Q_w^1, Q_w^{-1} , and Q_w^{-2} corresponding to thresholds $-3\kappa - \delta, -\kappa - \delta, \kappa - \delta$, and $3\kappa - \delta$. Each signal $Q_w^\ell, \dots, Q_w^1, Q_w^{-1}, \dots, Q_w^{-\ell}$ is a function of time. For better readability, we omit the function parameter t when it is clear from context.

Decision Separator. Any realistic hardware implementation of the offset measurement will have to account for setup/hold times of the registers it uses. We dedicate the decision separator ε to account for (small) additional setup/hold times, and the effect of a potentially metastable output in case a setup/hold time is violated. A visualization of the decision separator is given in Fig. 2.

We require that signal $Q_w^{\pm i}(t)$ is 1 at time t if the offset exceeds the i th threshold and we require that signal $Q_w^{\pm i}(t)$

is 0 at time t if the offset does not exceed the i th threshold. When the offset is close to the threshold (within ε), then we allow that $Q_w^{\pm i}(t)$ is unconstrained, i.e., $Q_w^{\pm i}(t) \in \{0, M, 1\}$, where M denotes a metastable or unstable value, e.g., a transition, a glitch, or a value between logical 0 and 1. Formally, we define the module's outputs to fulfill the following:

Definition 4.1 (decision separator). *Let ε be a (small) timespan with $\kappa \gg \varepsilon > 0$. At time t , we require the following constraints for all $i \in \{1, \dots, \ell\}$. Signal $Q_w^{\pm i}(t)$ is set to 1 if the offset estimate is larger than $\mp(2i - 1)\kappa - \delta$.*

$$\begin{aligned} \hat{O}_w(t) \geq -(2i - 1)\kappa - \delta &\Rightarrow Q_w^i(t) = 1 \\ \hat{O}_w(t) \geq (2i - 1)\kappa - \delta &\Rightarrow Q_w^{-i}(t) = 1 \end{aligned} \quad (\text{M1})$$

Signal $Q_w^{\pm i}(t)$ is set to 0 if the offset measurement is smaller than $\mp(2i - 1)\kappa - \delta - \varepsilon$.

$$\begin{aligned} \hat{O}_w(t) \leq -(2i - 1)\kappa - \delta - \varepsilon &\Rightarrow Q_w^i(t) = 0 \\ \hat{O}_w(t) \leq (2i - 1)\kappa - \delta - \varepsilon &\Rightarrow Q_w^{-i}(t) = 0 \end{aligned} \quad (\text{M2})$$

Otherwise, $Q_w^{\pm i}(t)$ is unconstrained, i.e., within $\{0, M, 1\}$.

Figure 3 (middle) shows the timing of signals $Q_w^{-1}(t)$, $Q_w^1(t)$, and $Q_w^2(t)$ in relation to the clock of neighbor w . When clk_v transitions to 1, the measurement module takes a snapshot of the outputs $Q_w^{\pm i}$. In Figure 3 (right), we show two examples.

Figure 3 (left) depicts transitions of the signals $Q_w^{\pm i}(t)$. The figure shows increasing \hat{O}_w (along the x -axis), resulting in more and more bits $Q_w^{\pm i}(t)$ flip to 1. The decision separator ε is small enough that no two bits can flip at the same time. If $\hat{O}_w(t) = 0$ we obtain $Q_w^i(t) = 1$ and $Q_w^{-i}(t) = 0$ for all $i \in \{0, \dots, \ell\}$.

Figure 3 (middle) also depicts transitions of the signals $Q_w^{\pm i}(t)$, but along the x -axis $L_v(t)$ increases while L_w is fixed. We mark time \mathcal{L}_w at which $L_v(t) = L_w$. A digital implementation is only able to measure the offset on a clock event, e.g., a rising clock transition. Hence, \mathcal{L}_w will be the time where clk_w rises. When $L_v(t) = L_w$, we have that $\hat{O}_w(t) = 0$, such that all bits $Q_w^i(t) = 1$ and $Q_w^{-i}(t) = 0$. As $L_v(t)$ increases, $\hat{O}_w(t)$ decreases. Hence, in Figure 3, (middle) is a mirror image of (left).

Example 4.2. Regarding Figure 3 (right), a measurement module with $\ell = 2$ can have output $Q_w(t) = 1100$ if $\kappa - \delta - \varepsilon \geq \hat{O}_w(t) \geq -\kappa - \delta$. The output may become $Q_w(t) = 11M0$ if $\kappa - \delta > \hat{O}_w(t) > \kappa - \delta - \varepsilon$.

In general, closely synchronized clocks have output $Q_w^{\pm i}(t) = 1^\ell 0^\ell$. If the clock of v is ahead of w 's clock, the measurement $Q_w^{\pm i}(t)$ contains more 0s than 1s. Similarly, if v 's clock is behind the clock of w , the outputs contain more 1s than 0s. Further, at most one output bit is M at a time if the ε -regions in Figures 3 (left) and (middle) do not overlap:

Lemma 4.3. *At every time t there is at most a single $i \in \{1, \dots, \ell\}$ such that $Q_w^{\pm i}$ is unconstrained.*

Proof. Assume for $i > 0$, that $Q_w^i(t)$ is unconstrained. Then we have that

$$-(2i - 1)\kappa - \delta - \varepsilon < \hat{O}_w(t) < -(2i - 1)\kappa - \delta.$$

Hence, for all $i' < i$ it holds that $\hat{O}_w(t) < -(2i' - 1)\kappa - \delta$, such that, by Definition 4.1, $Q_w^{i'} = 0$ and $Q_w^{-j} = 0$ for all

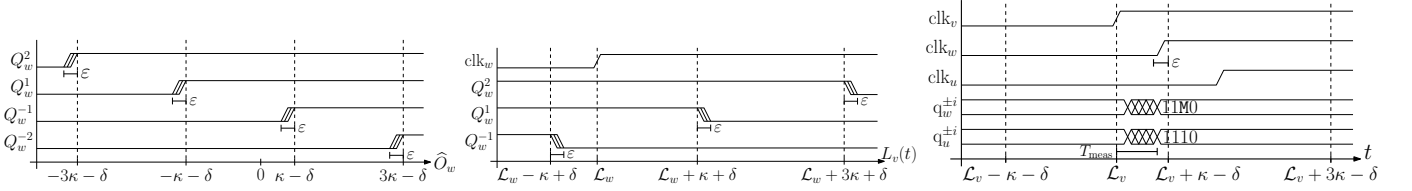


Fig. 3: Timing diagrams of the measurement module including the decision separator. (left) Output bits $Q_w^{\pm i}$ relative to the actual measurement $\hat{O}_w(t)$. (middle) Output bits $Q_w^{\pm i}(t)$ relative to the logical clock $L_w(t)$, assuming that $L_w(t)$ is known to v . (right) Example measurements from node v to nodes u and w , relative to Newtonian time t .

j . For all $i' > i$ we obtain $\hat{O}_w(t) > -(2i' - 1)\kappa - \delta - \varepsilon$, as $\kappa > \varepsilon$. Thus, by Definition 4.1, $Q_w^{i'} = 1$. An analogous argument shows that there is only one unconstrained bit if $Q_w^{-i}(t)$ is unconstrained. \square

Latency. Besides setup/hold times, we have to account further for propagation delays. Let T_{meas} denote the maximum end-to-end latency of the measurement module, i.e., an upper bound on the elapsed time from when $Q_w^{\pm i}(t)$ is set, to when the measurements are available at the output. More precisely, we require that if $Q_w^{\pm i}(t')$ is set to $x \in \{0, 1\}$ for all t' in $[t - T_{meas}, t]$, then the corresponding output $q_w^{\pm i}(t)$ is x as depicted in Figure 3 (right).

4.3 Control Module

Each node v is equipped with a control module. Its input is the (unary encoded) time measurement, i.e., bits $q_w^{\pm i}(t)$, for each of v 's neighbors. Output is the mode signal $md_v(t)$.

The control module is required to set the mode signal according to Algorithm OffsetGCS, i.e., to fast mode if FT is satisfied, otherwise the algorithm defaults to slow mode. Denote by T_{ctr} the maximum end-to-end delay of the control module circuit, i.e., the delay between its inputs (the measurement offset outputs) and its output $md_v(t)$. We then require the following: If OffsetGCS continuously maps the algorithm's switch $\gamma(t)$ to 0 for time T_{ctr} , then the output of the control module is 0 at time t :

$$\forall t' \in [t - T_{ctr}, t]. \gamma_v(t') = 0 \Rightarrow md_v(t) = 0. \quad (L1)$$

If OffsetGCS continuously maps the switch $\gamma(t)$ to 1 for time T_{ctr} , then the output of the control module is 1 at time t :

$$\forall t' \in [t - T_{ctr}, t]. \gamma_v(t') = 1 \Rightarrow md_v(t) = 1. \quad (L2)$$

Otherwise, the output is unconstrained, i.e., within $\{0, M, 1\}$.

Intuitively, FT triggers when there is an offset that crosses threshold i and no other offset is below threshold $-i$ for some $i \in \{1, \dots, \ell\}$. Hence, we select the maximum and minimum of the offsets $Q_w^{\pm i}$ to all neighbors w .

Since the network also includes self-loops (cf. Section 2), each node, conceptually, measures the offset to itself. The offset to self is always 0. In practice, that means that the maximum only needs to consider neighbors that are ahead and the minimum only needs to consider neighbors that are behind. For $i \in \{1, \dots, \ell\}$, signals $Q_w^{-i}(t)$ indicate whether node w is ahead and similar bits $Q_w^i(t)$ indicate whether w

is behind. Thus, the ℓ -bit encodings of maximum ($Q_{max}^{-i}(t)$) and minimum ($Q_{min}^i(t)$) are computed as

$$Q_{max}^{-i}(t) := \bigvee \{Q_w^{-i}(t) \mid w \text{ is neighbor of } v\},$$

$$Q_{min}^i(t) := \bigwedge \{Q_w^i(t) \mid w \text{ is neighbor of } v\}.$$

As FT is satisfied if $Q_{max}^{-i}(t)$ and $Q_{min}^i(t)$ are both 1 for any i in $\{1, \dots, \ell\}$. Signal $md_v(t)$ is computed by

$$md_v(t) := \bigvee \{Q_{max}^{-i} \wedge Q_{min}^i \mid i \in \{1, \dots, \ell\}\}.$$

Metastability-containment. Any metastability-containing implementation of $md_v(t)$ has the following properties: (i) If the slow condition is satisfied, then $md_v(t) = 0$ (ii) if the fast condition is satisfied, then $md_v(t) = 1$ (iii) if no condition is satisfied then $md_v(t)$ may output M . For a formal definition of metastability-containment, we refer the reader to [24]. In Section 5, we present a metastability-containing implementation of the control module.

4.4 ClockedGCS Algorithm

Clocked Algorithm. We are now in the position to assemble the modules into the so-called Clocked Gradient Clock Synchronization (ClockedGCS) algorithm (see Algorithm 3). In the following we prove Theorem 4.6, showing that the ClockedGCS algorithm implements the OffsetGCS algorithm, and hence maintains tight skew bounds. For the measurement module, we defined a possibly metastable assignment if the signal changes within an ε window during which it is assigned. We denote the assignment with propagation delay and possibly metastable result by \leftarrow_M .

Algorithm 3 Clocked algorithm ClockedGCS at v . The assignment \leftarrow_M denotes a possibly unstable assignment.

- 1: **at** each clock tick, at time t_{clk} **do**
- 2: **for** each $i \in \{1, \dots, \ell\}$ **do**
- 3: **for** each adjacent node w **do**
- 4: $q_w^i \leftarrow_M \hat{O}_w(t_{clk}) \geq -(2i - 1)\kappa - \delta$
- 5: $q_w^{-i} \leftarrow_M \hat{O}_w(t_{clk}) \geq (2i - 1)\kappa - \delta$
- 6: **at** each time t **do**
- 7: $q_{min}^i \leftarrow_M \bigwedge \{q_w^i(t) \mid w \text{ is neighbor of } v\}$
- 8: $q_{max}^{-i} \leftarrow_M \bigvee \{q_w^{-i}(t) \mid w \text{ is neighbor of } v\}$
- 9: $md_v \leftarrow_M \bigvee \{q_{min}^i(t) \wedge q_{max}^{-i}(t) \mid i \in \{1, \dots, \ell\}\}$

The ClockedGCS implements the OffsetGCS Algorithm. An essential difference of the ClockedGCS to the continuous time OffsetGCS algorithm is that measurements are

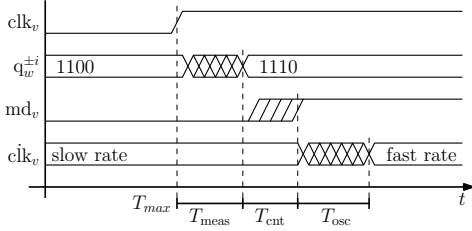


Fig. 4: Example timing diagram of the control module, depicting signals clk_v , $q_w^{\pm i}$, md_v and rate clk_v over Newtonian time t .

performed only at discrete clock ticks. We will, however, show that the clocked algorithm implements the OffsetGCS algorithm, with a properly chosen measurement error δ that accounts for the fact that we measure clock skew only at discrete points in time rather than continuously.

For that purpose, we denote the maximum end-to-end latency of the computation by T_{\max} . This end-to-end latency combines the delays of the three modules, i.e., $T_{\max} = T_{\text{meas}} + T_{\text{ctr}} + T_{\text{osc}}$. Thus, T_{\max} is the time it takes from a rising clock edge until the oscillator guarantees a stable rate. For a simple implementation, T_{\max} naturally becomes a lower bound on the clock period. Designs with a clock period beyond T_{\max} are possible when buffering measurements and mode signals.

Example 4.4. A timing diagram with the module outputs and the clock rate is given in Fig. 4. The offset measurement switches from 1100 (close to synchronous) to 1110 (v lagging behind w) and causes the oscillator to go to fast mode.

We are now in the position to relate the module delays to δ . We split δ into two parts, the *propagation delay uncertainty* and the *maximum end-to-end latency*. The propagation delay uncertainty accounts for variations in the time a signal takes to propagate from a node's oscillator to the measurement module of its neighbors. Suppose clock signals arrive at the measurement module with a larger or smaller delay than expected (usually due to variation in the fabrication process or environmental influences), then the module may measure larger or smaller offsets. We denote the propagation delay uncertainty by δ_0 .

The second source of error is the drift of the clocks when not measuring. The offset is measured once per clock cycle and it is used until the next measurement is made. During this time, the actual offset may change due to different modes and drift of oscillators. We denote the duration of a clock cycle (in slow mode with no drift) by T_{clk} . The maximum difference in rate between any two logical clocks is bounded by $(1 + \rho)(1 + \mu) - 1 = \rho + \mu + \rho\mu$. Thus, the maximum change of the offset during a clock cycle is at most

$$(\rho + \mu + \rho\mu)(T_{\text{clk}} + T_{\max}).$$

This is the second contribution to the uncertainty of the measurement. Summing up both contributions, the measurement error becomes

$$\delta = \delta_0 + (\rho + \mu + \rho\mu) \cdot (T_{\text{clk}} + T_{\max}).$$

Formally, we have the following:

Lemma 4.5. *Let $\delta = \delta_0 + (\rho + \mu + \rho\mu) \cdot T_{\text{clk}}$, then ClockedGCS satisfies Inequality (5) at all times t .*

Proof. The algorithm measures the offset $\hat{O}_w(t)$ at each clock tick. Hence, we show that between two clock ticks the uncertainty never grows beyond δ . Let t_{clk} and t'_{clk} be two consecutive clock ticks at node v . By the specification above, the measurement at time t_{clk} has precision δ_0 , such that

$$\left| \hat{O}_w(t_{\text{clk}}) - (L_w(t_{\text{clk}}) - L_v(t_{\text{clk}})) \right| \leq \delta_0.$$

During time interval $[t_{\text{clk}}, t'_{\text{clk}}] \leq T_{\text{ctr}}$ the clock rates may be different for neighbors. The difference between logical clocks grows at most by $(1 + \rho)(1 + \mu) \cdot T_{\text{clk}} - T_{\text{clk}} = (\rho + \mu + \rho\mu) \cdot T_{\text{clk}}$, such that for $t \in [t_{\text{clk}}, t'_{\text{clk}}]$,

$$\begin{aligned} & \left| \hat{O}_w(t) - (L_w(t) - L_v(t)) \right| \\ & \leq \left| \hat{O}_w(t_{\text{clk}}) - (L_w(t_{\text{clk}}) - L_v(t_{\text{clk}})) \right| + (\rho + \mu + \rho\mu) \cdot T_{\text{clk}} \\ & \leq \delta_0 + (\rho + \mu + \rho\mu) \cdot T_{\text{clk}}. \end{aligned}$$

Hence, at every time the error is at most δ , such that Inequality (5) is satisfied. \square

We are now in the position to prove the section's main result: under certain conditions on the algorithm's parameters, ClockedGCS implements OffsetGCS. If, in addition, the algorithm's parameters fulfill the conditions in Theorem 3.5, it follows that the skew bounds from the GCS algorithm apply to ClockedGCS.

Theorem 4.6. *Algorithm ClockedGCS is correct, i.e., it maintains the skew bounds in Theorem 3.4, if its parameters ε , δ_0 , and ρ fulfill constraints (C1)–(C4), (M1), (M2), (L1), and (L2) and parameters μ , κ , and ℓ are chosen according to Theorem 3.5.*

Proof. By choosing δ as in Lemma 4.5, Equation (5) is satisfied. A bounded local skew at all times $t \geq 0$ follows from (C1) and Theorem 3.5. This further implies the finiteness of parameter ℓ . For the correct choice of ℓ , lines 2–5 in ClockedGCS correspond to lines 2 and 3 of OffsetGCS according to (M1) and (M2). Given a metastability-containing implementation, line 7 (respectively 8) of ClockedGCS corresponds to line 4 (respectively 5) of OffsetGCS according to Boolean logic. Line 9 of ClockedGCS corresponds to lines 6–12 of OffsetGCS, where switching to fast (respectively slow) mode is ensured by (L1) and (C2) (respectively (L2) and (C3)). In case of a metastable assignment, (C4) ensures a correct behavior of the oscillator.

If constraints (C1)–(C4), (M1), (M2), (L1), and (L2) are fulfilled, then ClockedGCS implements OffsetGCS. By Theorem 3.5, every algorithm that implements OffsetGCS and satisfies the constraints in Theorem 3.5 maintains the skew bounds of Theorem 3.4. \square

5 HARDWARE IMPLEMENTATION

We next present a hardware implementation of the ClockedGCS algorithm, which we refer to as GCSoc. We then discuss its performance and how the system's parameters affect the achieved skews. For the latter, we designed an ASIC in the 15 nm FinFET-based NanGate OCL [19] technology. The design is laid out and routed with Cadence Encounter, which is also used for the extraction of parasitics

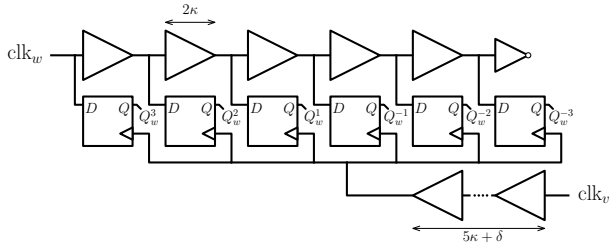


Fig. 5: Schematic of the time offset measurement module for $\ell = 3$.

and timing. Local clocks run at a frequency of approximately 2 GHz, controllable within a factor of $1 + \mu \approx 1 + 10^{-4}$. We use a larger factor μ to make the interplay of ρ and μ better visible. We compile two systems of 4 respectively. 7 nodes connected in a line. To resemble a realistically sparse spacing of clock regions, we placed nodes at distances of 200 μm . Hence, the PALS systems shown in the simulations are designed to cover floorplans of width 200 μm and length 800 μm respectively 1.4 mm.

Offset Measurement. Figure 5 shows a linear TDC-based circuitry for the module which measures the time offsets between nodes v and w . Buffers are used as delay elements for incoming clock pulses. The offset is measured in steps of 2κ , hence, buffers in the upper delay line have a delay of 2κ . The delay line is tapped after each buffer for corresponding $Q_w^{\pm i}$. A chain of flip-flops takes a snapshot of the delay line by sampling the taps. We require $Q_w^{-i} = 0$ and $Q_w^i = 1$, for all i , when $\hat{O}_w \geq -\kappa - \delta$ and $\hat{O}_w \leq \kappa - \delta - \varepsilon$ according to (M1) and (M2). Thus, we delay clk_v by $5\kappa + \delta + \varepsilon$. The decision separator ε accounts for the critical setup/hold window of the flip-flop.

Example 5.1. If both clocks are perfectly synchronized, i.e., $L_v = L_w$, then the state of the flip-flops will be $Q_w^3 Q_w^2 Q_w^1 Q_w^0 Q_w^{-1} Q_w^{-2} Q_w^{-3} = 111000$ after a rising transition of clk_v . Now, assume that clock w is ahead of clock v , say by a small $\varepsilon > 0$ more than $\kappa + \delta$, i.e., $L_w = L_v + \kappa - \delta + \varepsilon$. For the moment assuming that we do not make a measurement error, we get $\hat{O}_w = L_w - L_v = \kappa - \delta + \varepsilon$. From the delays in Fig. 5 one verifies that in this case, the flip-flops are clocked before clock w has reached the second flip-flop with output Q_w^1 , resulting in a snapshot of 110000. Likewise, an offset of $\hat{O}_w = L_w - L_v = 3\kappa - \delta + \varepsilon$ results in a snapshot of 100000.

Control Module. Given node v 's time offsets to its neighbors in unary encoding, the control module computes the minimal and maximal threshold levels which have been reached. The circuit in Figure 6 implements the control module for 3 neighbors w_1, w_2 , and w_3 . As described in Section 4.3, we only need to compute the maximal value of bits Q_w^{-i} and the minimal value of bits Q_w^i ; which can be easily computed by an `or` respectively `and` over all neighbors.

Given the maximal and minimal values, the circuit in Fig. 6b computes FT and sets md_v to 1 if it holds.

Metastability-Containing Control Module. As described in Section 4, the inputs to the control module may be metastable, i.e., unknown or even oscillating signals between ground and supply voltage. It remains for us to

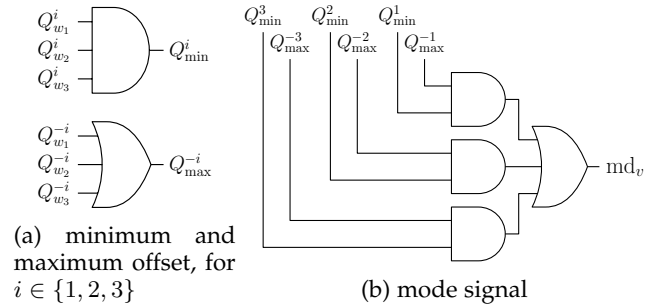


Fig. 6: Schematics of the control module for three neighbors (w_1, w_2 , and w_3).

show that the control module, given in Figure 6, fulfills specifications (L1) and (L2). In particular, we need to ensure that the specifications are met for metastable inputs.

The circuit in Figure 6 follows from the definition of md_v in Section 4.3, when replacing each conjunction (respectively disjunction) by an `and` (respectively `or`) gate. Due to the masking properties of `and` and `or` gates, the output md_v can only become metastable when there is an i such that one of Q_{\min}^i or Q_{\max}^{-i} is M and the other is 1 or M. This is only the case when Eq. (L1) and Eq. (L2) do not apply. It follows that the output of the control module can only become metastable when the mode signal is unconstrained and the conditions are met.

Tunable Oscillator. As a local clock source, we use a ring oscillator inspired by the starved inverter ring presented in [25]. We use a ring of inverters, where some inverters being current-starved-inverters, to set the frequency to either fast mode or slow mode. Nominal frequency is around 2 GHz, controllable by a factor $1 + \mu \approx 1 + 10^{-4}$ via the md_v signal. For our simulations, we choose $\rho \approx \mu/10 \approx 10^{-5}$, assuming a stable oscillator. While this requirement poses a challenge to an oscillator design, it can be relaxed in different ways: (i) By choosing larger parameters μ and ρ such that their ratio remains fixed, i.e., $\mu/\rho = 10$, this forces us to choose a larger κ , and hence requires to measure larger time offsets. This is at the cost of a larger skew and circuit (this follows from combining Theorem 3.4, Theorem 3.5, and Lemma 4.5). (ii) By locking the local oscillators to a central quartz oscillator. The problem is different from building a balanced clock tree since the quartz's skew can be neglected here. (iii) We conjecture that with a refined analysis of the algorithm: rather than absolute drift, the drift with respect to a neighboring oscillator is determinant. Neighboring oscillators show reduced drift due to common cause effects.

The tunable ring oscillator comes with the advantage that for any input voltage it runs at a speed between fast and slow mode, hence, (C4) is satisfied. In the following paragraph, we define an upper bound on T_{osc} such that constraints (C2) and (C3) are satisfied.

Timing Parameters. We next discuss how the modules' timing parameters relate to the extracted physical timing of the above design.

The time T_{osc} required for switching between oscillator modes is about the delay of the ring oscillator, which in our case is about $1/(2 \cdot 2 \text{ GHz}) = 250 \text{ ps}$. An upper bound on the measurement latency (T_{meas}) plus the controller latency

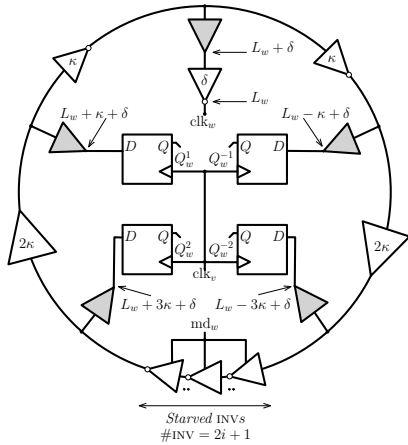


Fig. 7: Schematic of the improved offset measurement implementation. Node v 's offset measurement is integrated into w 's ring oscillator. Labels of the delay elements denote their delay. We also annotate the measured phase offsets.

(T_{ctr}) is given by a clock cycle (500 ps) plus the delay (25 ps) of the circuitry in Figure 6. In our case, delay extraction of the circuit yields $T_{\text{meas}} + T_{\text{ctr}} < 500 \text{ ps} + 25 \text{ ps}$. We thus have, $T_{\text{max}} < T_{\text{meas}} + T_{\text{ctr}} + T_{\text{osc}} = 775 \text{ ps}$.

The uncertainty, δ_0 , in measuring if \hat{O}_w has reached a certain threshold is given by the uncertainties in latency of the upper delay chain plus the lower delay chain in Fig. 5. For the described naive implementation using an uncalibrated delay line, this would be problematic: Extracting delays from the design after layout, the constraints from Definition 3.5 were met for delay uncertainties of $\pm 1\%$, but not for the $\pm 5\%$ we targeted. We thus redesigned the Offset Measurement circuit as described in the following.

Improved Offset Measurement. Figure 7 shows an improved TDC-type offset measurement circuit that does not suffer from the problem above. Conceptually, the TDC of the node v that measures offsets w.r.t. node w is integrated into the local ring oscillator of the neighboring node w . If w has several neighbors, e.g., up to 4 in a grid, they share the taps but have their own flip-flops within the node w .

Figure 7 presents a design for $\ell = 2$ with 4 taps and a single neighbor v . In our hardware implementation we set $\ell = 2$, as even for $\mu/\rho = 10$ this is sufficient for networks of diameter up to around 80 (see how to choose this set of thresholds in the specification of this module in Section 4). The gray buffers at the offset measurement taps decouple the load of the remaining circuitry. At the bottom of the ring oscillator, an odd number of starved inverters are used to set the slow or fast mode for node w . The delay elements at the top are inverters instead of buffers to achieve a latency of $\kappa = 10 \text{ ps}$. We inverted the clock output to account for the negated signal at the tap of clock w at the top.

When integrating the measurement into the ring oscillator, the constraints (C2)–(C4) and (M1), (M2) are still met for a suitable choice of T_{osc} . Integration of the TDC into w 's local ring oscillator greatly reduces uncertainties at both ends: (i) the uncertainty at the remote clock port (of node w) is removed to a large extent since the delay elements which are used for the offset measurements are part of w 's

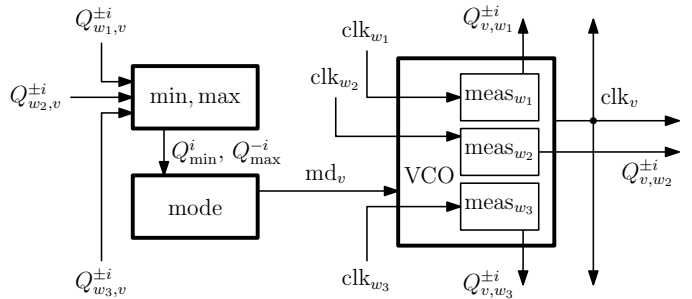


Fig. 8: Schematic of a node v with neighbors w_1 , w_2 , and w_3 , using the improved offset measurement integrated in the VCO. Note that measurement $Q_{a,b}^{\pm i}$ is the difference between nodes a and b , as measured by b .

oscillator, and (ii) the uncertainty at the local clock port is greatly reduced by removing the delay line of length $5\kappa + \delta$. The remaining timing uncertainties are the latency from taps to the D-ports of the flip-flops and from clock v to the clk_v -ports of the flip-flop. Timing extraction yielded $\delta_0 < 4 \text{ ps}$ in presence of $\pm 5\%$ gate delay variations.

Full Hardware Implementation. We depict in Fig. 8 the schematic of a node with three neighbors. From Theorem 3.5, we obtain $\kappa \approx 10 \text{ ps}$ and $\delta \approx 5 \text{ ps}$ which matched the previously chosen latencies of the delay elements. Applying Theorem 3.4, finally, yields the global and local skew bounds: $\mathcal{G}(t) \leq 1.223\kappa D = 12.23D \text{ ps}$ and $\mathcal{L}(t) \leq (\lceil \log_{10}(1.223D) \rceil + 1)\kappa$. For our design with diameter $D = 3$ this makes a maximum global skew of 36.69 ps and a maximum local skew of $2\kappa = 20 \text{ ps}$. With regard to diameter $D = 6$, we obtain a maximum global skew of 73.38 ps and a maximum local skew of $2\kappa = 20 \text{ ps}$.

As described above, GCSoc satisfies constraints (C2) – (C4), (M1), (M2), (L1), and (L2). Parameters ε , δ_0 , and ρ are restricted by the technology. For our choices of ℓ , μ , and κ GCSoc satisfies the conditions of Theorem 3.5. Thus, from Theorem 4.6 it follows that our implementation maintains the skew bounds of the GCS algorithm.

Corollary 5.2. *Given (C1), GCSoc is an implementation of ClockedGCS. Hence, it maintains global skew $\mathcal{G}(t) \leq \mathcal{O}(\delta D)$ and local skew $\mathcal{L}(t) \leq \mathcal{O}(\delta \log_{\mu/\rho} D)$.*

Remark. (i) Note that this section gives a “recipe” for realizing a GCSoc system for any network, e.g., how the hardware parameters affect the local and global skews. Also note that because a GCSoc system implements a ClockedGCS algorithm, all skews are provably and deterministically guaranteed.

(ii) Considerably larger systems, e.g., a grid with side length of $W = 32$ nodes and diameter $D = 2W - 2 = 62$, still are guaranteed to have a maximum local skew of $2\kappa = 20 \text{ ps}$. If we choose $\mu = 10^{-3}$, the base of the logarithm in the skew bound increases from 10 to 100.

6 SIMULATIONS

We ran SPICE simulations of the post-layout extracted design with Cadence Spectre. Simulated systems had 4 and 7 nodes arranged in a line, as described in Section 5. We chose

a line setup since it allows us to compare local (between neighbors) versus global (typically the line ends) skew best. Nodes are labeled 0 to 3 (respectively 6). For the simulations, we set $\mu = 10\rho$ (instead of 100ρ), resulting in a slower decrease of skew, to observe better how the skew is removed. Operational corners of the SPICE simulations were 0.8 V supply voltage and 27 °C temperature.

Simulation with a small initial skew yields a peak power of 20.25 mW during stabilization and an average power of 5.26 mW. The performance measure of our system is given by the quality of the local skew. We discuss in detail the local skew for different set-ups in the next section.

6.1 SPICE Simulations on a 4 Node Topology

Scenarios. We designed three simulation scenarios with different initial skews that demonstrate different properties of the algorithm: *AHEAD*: node 1 is initialized with an offset of 40 ps ahead of all other nodes, *BEHIND*: node 1 is initialized with an offset of 40 ps behind all other nodes, and *GRADIENT*: nodes are initialized with small skews on each edge, that sum up to a large 105 ps global skew. Simulation time for all scenarios is 1000 ns (≈ 2000 clock cycles).

Figure 9a depict the local and global skews of all scenarios. Observe that all local skews decrease until they reach less than 9 ps. The local skew then remains in a stable region. This is well below our worst-case bound of 20 ps on the local skew. We observe that the global skew slightly increases at the beginning of scenario *AHEAD* and after roughly 500 ns in scenario *BEHIND*.

One Node Ahead. Figure 10 shows the clock signals of nodes 0 to 3 at three points in time for scenario *AHEAD*: (i) shortly after the initialization, (ii) around 100 ns, and (iii) after 175 ns. The skews on the three nodes' edges are depicted in Fig. 9b.

For the mode signals, in the first scenario, we observe the following: Since node 1 is ahead of nodes 0 and 2, node 1's mode signal is correctly set to 0 (slow mode) while node 0 and 2's mode signals are set to 1 (fast mode). Node 3 is unaware that node 1 is ahead since it only monitors node 2. By default, its mode signal is set to slow mode. Node 2 then advances its clock faster than node 3. When the gap between 2 and 3 is large enough, node 3 switches to fast mode. This configuration remains until nodes 0 and 2 catch up to node 1, where they switch to slow mode not to overtake node 1. Again, node 3 sees only node 2, which is still ahead, and switches to slow mode only after it catches up to 2.

One Node Behind. The skews on the edges (0,1), (1,2), and (2,3) are depicted in Fig. 9c. We plot the absolute value of the skew, e.g., at roughly 500 ns node 1 overtakes node 0. The simulation shows that the algorithm immediately reduces the local skew. After the system reaches a small local skew after 200 ns, nodes drift relative to each other, e.g., node 2 drifts ahead of node 3, and node 1 overtakes node 0. The local skew remains in the stable (oscillatory) state after 200 ns and does not increase significantly.

Gradient Skew. The scenario *GRADIENT* demonstrates how the *OffsetGCS* algorithm works. It reduces the local skew in steps of (odd multiples of) κ , as seen in the plot in Fig. 9d

that looks like a staircase. The algorithm reduces skew on one edge at a time until it reaches the next plateau.

Figure 9d demonstrates how skew is removed. *OffsetGCS* starts by reducing skew on edge (1,2) until it reaches the plateau of (0,1) and (2,3). One by one it then reduces skew on edges (0,1), (1,2) to (2,3) until they reach the next plateau. Finally, it reduces the skews one by one (in reverse order) down to a stable range. Figure 11 shows the same trace in a plot similar to Fig. 1.

Remark. For the sake of a clearly visible convergence of the skew over time, we chose initial skews that are beyond the bound in (C1). Thus, the weaker self-stabilizing bound from Theorem 3.4 applies. All simulations showed convergence to a small local skew despite the less conservative initialization – demonstrating the robustness of our algorithm also to larger initial skews. For our stronger bounds to hold, the reader may consider only a respective postfix of the simulation.

6.2 Process Variations

In order to show resilience of our implementation towards process variations, we introduce variations to the extracted netlist and run further SPICE simulations. We initialize node 1 with a small offset to nodes 0, 2, and 3. Variations affect the width and length of n-channel and p-channel transistors and the supply voltage, where all parameters are simulated at 90%, 100%, and 110% of their typical value. The resulting skew on edge (0,1) for each simulation is depicted in Fig. 12. The simulations show that our system performs well even under process variations. The local skew after stabilization is below the theoretical bound of 20 ns.

6.3 Comparison to a Clock Tree

For comparison, we laid out a grid of $W \times W$ flip-flops, evenly spread in 200 μm distance in x and y direction across the chip. The data port of a flip-flop is driven by the `OR` of the up to four adjacent flip-flops. Clock trees were synthesized and routed with Cadence Innovus, with the target to minimize skews. Parameters for delay variations on gates and nets were set to $\pm 5\%$.

For a 2×2 grid, Innovus reported an area of 1.48 μm^2 and power of 0.231 mW for the clock tree. Reported numbers for the PALS system, which comprises 4 nodes in a line, are 67.09 μm^2 area and 0.023 mW power. Numbers for the PALS system do not include the 4 starved inverter ring oscillators. We point out that the size of 67.09 μm^2 covers only 0.04% of the floorplan. The PALS system uses 171 gates from the standard cell library.

The resulting clock skews are presented in Fig. 13. We plotted skews guaranteed by our algorithm for the same grids with parameters extracted from the implementation described in Section 5. Observe the linear growth of the local clock skew measured in the simulation compared to the logarithmic growth of the analytical upper bound on the local skew in our implementation. The figure also shows the simulated skew for a clock tree with delay variations of $\pm 10\%$. This comparison is relevant, as δ_0 is governed by *local* delay variations, which can be expected to be smaller than those across a large chip.

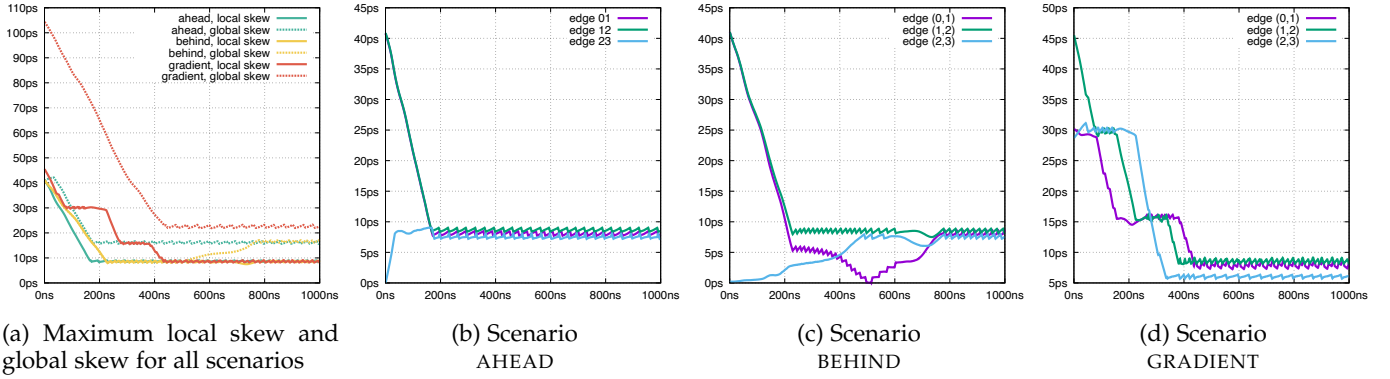


Fig. 9: Skews on edges (0, 1), (1, 2), and (2, 3) in the 4 node topology, showing the skew (y-axis) over simulated time (x-axis) for SPICE simulations of scenarios AHEAD, BEHIND, and GRADIENT.

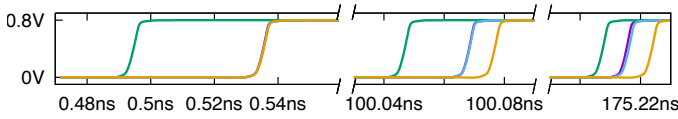


Fig. 10: Excerpt of scenario AHEAD. Clock signals of node 0 (purple), 1 (green), 2 (blue), and 3 (yellow). We show voltage of the clk signals on the x-axis over simulated time on the y-axis. Nodes from left to right: (i) 1 before 0, 2, 3, (ii) 1 before 0, 2 before 3, (iii) 1 before 0, 0 slightly before 2, 2 before 3.

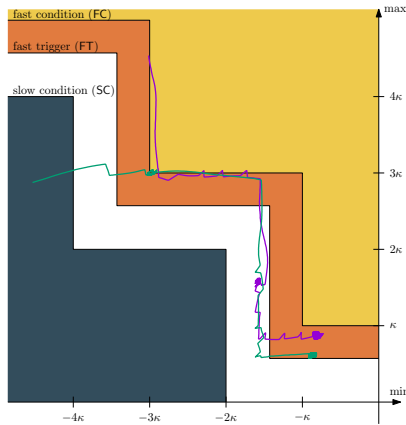


Fig. 11: Simulated trajectory of \hat{O}_{\max} and \hat{O}_{\min} of node 1 (purple) and node 2 (green) from scenario GRADIENT plotted in Fig. 1

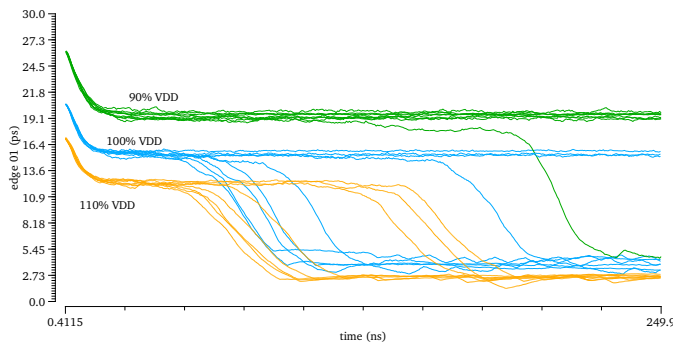


Fig. 12: Simulation results for skew (y-axis) over simulated time (x-axis) for edge (0, 1) under 90%, 100%, and 110% variation of the supply voltage and transistor sizes.

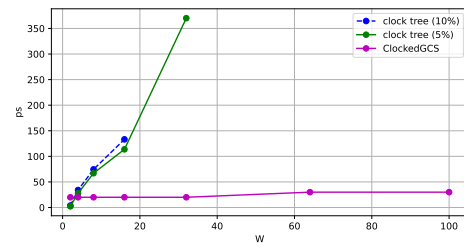


Fig. 13: Local skew (ps) between neighboring flip-flops in the $W \times W$ grid, with unit length $200 \mu\text{m}$. Clock tree with $\pm 5\%$ delay variation (solid green) and our algorithm with $\pm 5\%$ delay variation (solid magenta). The dotted line shows the clock tree with $\pm 10\%$ delay variation, demonstrating linear growth of the skew also in a different setting. Clock trees are shown up to $W = 32$ (i.e., floorplan of width and length 6.4 mm) after which Innovus ran out of memory.

While a priori the observed linear local skew may be due to the tool, it has been shown that no tool can obtain a local skew less than proportional to W [26]. This follows from the fact that there are always two neighboring nodes in the grid which are in distance proportional to W from each other in the clock tree [26], [27]. Accordingly, uncertainties accumulate in the worst-case fashion to create a local skew which is proportional to W . Our algorithm, on the other hand, manages to reduce the local skew exponentially to being proportional to $\log W$.

To gain intuition on this result, note that there is always an edge that, if removed (see the edge which is marked by an X in Fig. 14), partitions the tree into two subtrees each spanning an area of $\Omega(W^2)$ and hence having a shared perimeter of length $\Omega(W)$. Thus, there must be two adjacent nodes, one on each side of the perimeter, at distance $\Omega(W)$ in the tree.

6.4 Comparison to Distributed Clock Generation

We next compare our findings to distributed clock generation schemes. Natural are *wait-for-all* and *wait-for-one*, where a node produces its next clock tick once it receives a tick by one or all its neighbors. Both approaches are vulnerable to large local skews, however.

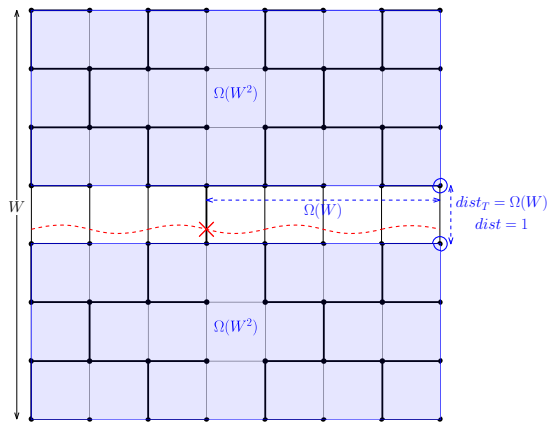


Fig. 14: A low stretch spanning tree of an $W \times W$ ($W = 8$) grid [28]. The bold lines depict the spanning tree, i.e., our clock tree in this example. The two neighboring nodes that are of distance 13 in the tree are circled (at the middle right side of the grid).

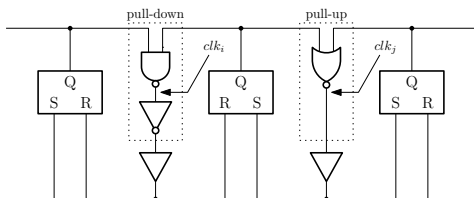


Fig. 15: Schematic of the digital abstraction of the Fairbanks clock generation on a line showing one pull-down and one pull-up node.

A clever combination of both schemes is used by the clock generation grid by Fairbanks and Moore [17]. In the grid, both approaches alternate for adjacent nodes. For comparison, we simulated a digital abstraction of the clock generation grid. Based on ideas of the lower bound proof for local skews [29], we construct a simulation scenario that demonstrates that large local skew are possible in the clock grid, however.

Clock Generation Grid. The clock generation grid is a self-timed analog circuit that provides local, synchronized clocks. It is based on the *Dynamic asP* FIFO control by Molnar and Fairbanks [30]. While the optimized version of the clock generation grid is an analog implementation that involves rigorous transistor sizing and layout, we focus on a digital version [17] which is easier to adapt and manufacture in a standard design process. We distinguish two types of nodes: pull-up nodes and pull-down nodes (see Fig. 15). On every edge between two nodes, there is a set-reset latch. Pull-up nodes set the latch and pull-down nodes reset the latch. Pull-up nodes compute the logical *nor* of incoming edges (equivalent to a wait-for-all approach) and set the latch. Pull-down nodes compute the logical *and* of incoming edges (equivalent to a wait-for-one approach) and reset the latch. The clock of a node is derived by the output of the respective *nor* or *and*. The grid’s frequency is easily adjusted by adding a delay between the nodes and the latches.

Setup. We next conducted simulations that examine the

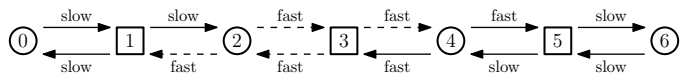


Fig. 16: Delay setup with fast and slow message delays for the Fairbanks clock generation on a line. The setup achieves a large local skew. Round nodes denote pull-down nodes and rectangular nodes denote pull-up nodes. In the lower bound simulation dashed edges are swapped from fast to slow communication.

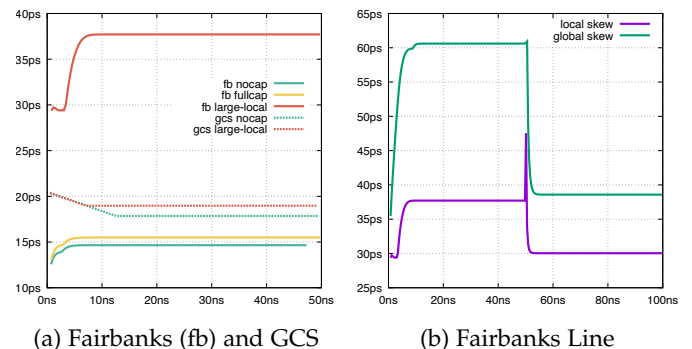


Fig. 17: Comparison of Fairbanks to ClockedGCS. (a) Local skews of the experiments NOCAP, FULLCAP, and LARGE-LOCAL. (b) Local and global skew of the lower bound simulation.

behavior of different communication delays. In order to simulate slower communication paths, we add a small capacity (0.01 pF) to the communication channel. For simplicity, we differentiate between two delays: fast and slow.

Formally, the algorithm combining wait-for-all and wait-for-one approaches can have a local skew that grows linearly with the network diameter. Through our simulations, we demonstrate that this is indeed possible in the clock generation grid and that *OffsetGCS* can cope with this situation. The setup of the simulated delays is depicted in Fig. 16: outgoing edges of nodes 2, 3, and 4 are fast and edges outgoing from 0, 1, 5, and 6 are slow.

Results for Clock Generation Grid. The digital clock generation grid runs at a frequency of about 2.5 GHz. By simulations, we determined that an additional capacity of 0.01 pF on an edge adds a delay of approximately 7 ps. We next conducted simulations with three different delay settings: NOCAP: the grid without additional delays, FULLCAP: the grid with the capacity added to every edge, and LARGE-LOCAL: the grid with the setting from Fig. 16.

Local skews of simulation scenarios NOCAP, FULLCAP, and LARGE-LOCAL are shown in Fig. 17a. We observe that the grid achieves a low skew if the delay is uniform on all edges. For scenario NOCAP (respectively. FULLCAP) we measure a local skew of 15 ps (respectively. 16 ps) and global skew of 22 ps (respectively. 23 ps). By contrast, the grid experiences poor synchronization for non-uniform delays (LARGE-LOCAL) where we obtained a local skew of 38 ps and a global skew of 61 ps.

Lower Bound Simulation. In this simulation, we apply ideas from the formal argument for lower bounds on wait-for-all and wait-for-one approaches. The idea is to build up

a large global skew and then change the edges' delays step by step, pushing the global skew onto a single edge. The simulation in Fig. 17b shows one of these push-steps. In the first part of the simulation (until 50 ns) the system builds up a large local skew. At 50 ns we switch delays of edges outgoing from nodes 3 and 4 as described in Fig. 16. As expected, the global skew is pushed onto the local skew right after (we measure 47 ps). Following the argument of the lower-bound proof, one can repeat the procedure to push the complete global skew (temporarily) onto a single edge.

Comparison to GCSoc. Our clock generation algorithm runs at a frequency of about 2 GHz. By simulations, we measured that the added capacity of 0.01 pF adds a delay of approximately 1 ps. We observed a local skew of 18 ps and a global skew of 20 ps in the absence of additional communication delay. This is slightly worse than the local skew of the grid (see Fig. 17a). However, by our theoretical findings, our algorithm does not suffer from a large skew in the setting where delays in the center are fast or switched from fast to slow: simulations of Fig. 16 showed a local skew of 19 ps and a global skew of 20 ps.

7 CONCLUSION

The presented ClockedGCS algorithm is a clock synchronization algorithm that provably maintains the skew bounds of the GCS algorithm by Lenzen et al. [18]. The algorithm can be deconstructed into parts that hardware modules can implement. Asymptotically, the algorithm maintains a local skew that is at most logarithmic in the chip's width, whereas clock trees are shown to perform only linear in the width of the chip.

By simulation, we show that our GCSoc implementation of these modules in a 15 nm FinFET achieves small skews between neighbors even under process variations. We discuss different simulation setups that show how the algorithm behaves.

In future work, we aim to improve the analysis of the GCS algorithm by showing its correctness for oscillators with less stringent requirements. Additionally, we plan to conduct simulations of a full design, incorporating PVT and PPA experiments, and eventually produce an ASIC chip for comparison to a cutting-edge GALS design.

ACKNOWLEDGMENTS

The authors would like to thank the team of EnICS Labs for support and helpful discussions. In particular, we thank Benjamin Zambrano and Itamar Levi, Itay Merlin, Shawn Ruby, Adam Teman, Leonid Yavits. This project has received funding from the European Research Council (ERC) under the European Union's Horizon 2020 research and innovation programme (grant agreement 716562). This research was supported by the Israel Science Foundation under Grant 867/19 and by the ANR project DREAMY (ANR-21-CE48-0003).

REFERENCES

- [1] J. Bund, M. Függer, C. Lenzen, M. Medina, and W. Rosenbaum, "PALS: plesiochronous and locally synchronous systems," in *26th IEEE International Symposium on Asynchronous Circuits and Systems, ASYNC 2020, Salt Lake City, UT, USA, May 17-20, 2020*. IEEE, 2020, pp. 36–43. [Online]. Available: <https://doi.org/10.1109/ASYNC49171.2020.00013>
- [2] H. D. Foster, "Trends in functional verification: a 2014 industry study," in *Proceedings of the 52nd Annual Design Automation Conference, San Francisco, CA, USA, June 7-11, 2015*. ACM, 2015, pp. 48:1–48:6. [Online]. Available: <https://doi.org/10.1145/2744769.2744921>
- [3] A. J. Martin, "Compiling communicating processes into delay-insensitive VLSI circuits," *Distributed Comput.*, vol. 1, no. 4, pp. 226–234, 1986. [Online]. Available: <https://doi.org/10.1007/BF01660034>
- [4] —, "The limitations to delay-insensitivity in asynchronous circuits," in *Beauty is our business*. Springer, 1990, pp. 302–311.
- [5] R. Manohar and Y. Moses, "The eventual c-element theorem for delay-insensitive asynchronous circuits," in *23rd IEEE International Symposium on Asynchronous Circuits and Systems, ASYNC 2017, San Diego, CA, USA, May 21-24, 2017*. IEEE Computer Society, 2017, pp. 102–109. [Online]. Available: <https://doi.org/10.1109/ASYNC.2017.15>
- [6] —, "Asynchronous signalling processes," in *25th IEEE International Symposium on Asynchronous Circuits and Systems, ASYNC 2019, Hiroasaki, Japan, May 12-15, 2019*. IEEE, 2019, pp. 68–75. [Online]. Available: <https://doi.org/10.1109/ASYNC.2019.00018>
- [7] D. M. Chapiro, "Globally-asynchronous locally-synchronous systems." Stanford Univ CA Dept of Computer Science, Tech. Rep., 1984.
- [8] P. Teehan, M. R. Greenstreet, and G. G. Lemieux, "A survey and taxonomy of GALS design styles," *IEEE Des. Test Comput.*, vol. 24, no. 5, pp. 418–428, 2007. [Online]. Available: <https://doi.org/10.1109/MDT.2007.151>
- [9] R. R. Dobkin, R. Ginosar, and C. P. Sotiriou, "Data Synchronization Issues in GALS SoCs," in *10th International Symposium on Advanced Research in Asynchronous Circuits and Systems (ASYNC 2004), 19-23 April 2004, Crete, Greece*. IEEE Computer Society, 2004, pp. 170–180. [Online]. Available: <https://doi.org/10.1109/ASYNC.2004.1299298>
- [10] L. R. Dennison, W. J. Dally, and T. Xanthopoulos, "Low-latency plesiochronous data retiming," in *16th Conference on Advanced Research in VLSI (ARVLSI '95), March 27-29, 1995, Chapel Hill, North Carolina, USA*. IEEE Computer Society, 1995, pp. 304–315. [Online]. Available: <https://doi.org/10.1109/ARVLSI.1995.515628>
- [11] A. Chakraborty and M. R. Greenstreet, "Efficient self-timed interfaces for crossing clock domains," in *9th International Symposium on Advanced Research in Asynchronous Circuits and Systems (ASYNC 2003), 12-16 May 2003, Vancouver, BC, Canada*. IEEE Computer Society, 2003, pp. 78–88. [Online]. Available: <https://doi.org/10.1109/ASYNC.2003.1199168>
- [12] K. Y. Yun and R. P. Donohue, "Pausible clocking: A first step toward heterogeneous systems," in *1996 International Conference on Computer Design (ICCD '96), VLSI in Computers and Processors, October 7-9, 1996, Austin, TX, USA, Proceedings*. IEEE Computer Society, 1996, pp. 118–123. [Online]. Available: <https://doi.org/10.1109/ICCD.1996.563543>
- [13] X. Fan, M. Krstic, and E. Grass, "Analysis and optimization of pausable clocking based GALS design," in *27th International Conference on Computer Design, ICCD 2009, Lake Tahoe, CA, USA, October 4-7, 2009*. IEEE Computer Society, 2009, pp. 358–365. [Online]. Available: <https://doi.org/10.1109/ICCD.2009.5413130>
- [14] M. Függer and U. Schmid, "Reconciling fault-tolerant distributed computing and systems-on-chip," *Distributed Comput.*, vol. 24, no. 6, pp. 323–355, 2012. [Online]. Available: <https://doi.org/10.1007/s00446-011-0151-7>
- [15] D. Dolev, M. Függer, U. Schmid, and C. Lenzen, "Fault-tolerant algorithms for tick-generation in asynchronous logic: Robust pulse generation," *Journal of the ACM (JACM)*, vol. 61, no. 5, p. 30, 2014.
- [16] T. C. Fischer, A. K. Nivarti, R. Ramachandran, R. Bharti, D. Carson, A. Lawrendra, V. Mudgal, V. Santhosh, S. Shukla, and T.-C. Tsai, "9.1 D1: A 7nm ML training processor with wave clock distribution," in *2023 IEEE International Solid-State Circuits Conference (ISSCC)*. IEEE, 2023, pp. 8–10.

- [17] S. Fairbanks and S. W. Moore, "Self-timed circuitry for global clocking," in *11th International Symposium on Advanced Research in Asynchronous Circuits and Systems (ASYNC 2005)*, 14-16 March 2005, New York, NY, USA. IEEE Computer Society, 2005, pp. 86–96. [Online]. Available: <https://doi.org/10.1109/ASYNC.2005.29>
- [18] C. Lenzen, T. Locher, and R. Wattenhofer, "Tight bounds for clock synchronization," *J. ACM*, vol. 57, no. 2, pp. 8:1–8:42, 2010. [Online]. Available: <https://doi.org/10.1145/1667053.1667057>
- [19] M. G. A. Martins, J. M. Matos, R. P. Ribas, A. I. Reis, G. Schlinker, L. Rech, and J. Michelsen, "Open cell library in 15nm freepdk technology," in *Proceedings of the 2015 Symposium on International Symposium on Physical Design, ISPD 2015, Monterey, CA, USA, March 29 - April 1, 2015*, A. Davoodi and E. F. Y. Young, Eds. ACM, 2015, pp. 171–178. [Online]. Available: <https://doi.org/10.1145/2717764.2717783>
- [20] L. R. Marino, "General theory of metastable operation," *IEEE Trans. Computers*, vol. 30, no. 2, pp. 107–115, 1981. [Online]. Available: <https://doi.org/10.1109/TC.1981.6312173>
- [21] J. Bund, M. Függer, C. Lenzen, M. Medina, and W. Rosenbaum, "PALS: plesiochronous and locally synchronous systems," *CoRR*, vol. abs/2003.05542, 2020. [Online]. Available: <https://arxiv.org/abs/2003.05542>
- [22] D. Konstantinou, A. Psarras, C. Nicopoulos, and G. Dimitrakopoulos, "The mesochronous dual-clock fifo buffer," *IEEE Transactions on Very Large Scale Integration (VLSI) Systems*, vol. 28, no. 1, pp. 302–306, 2019.
- [23] J. Bund, M. Függer, C. Lenzen, and M. Medina, "Synchronizer-free digital link controller," *IEEE Transactions on Circuits and Systems I: Regular Papers*, vol. 67, no. 10, pp. 3562–3573, 2020.
- [24] S. Friedrichs, M. Függer, and C. Lenzen, "Metastability-containing circuits," *IEEE Trans. Computers*, vol. 67, no. 8, pp. 1167–1183, 2018. [Online]. Available: <https://doi.org/10.1109/TC.2018.2808185>
- [25] D. Ghai, S. P. Mohanty, and E. Kougianos, "Design of parasitic and process-variation aware Nano-CMOS RF circuits: A VCO case study," *IEEE Trans. Very Large Scale Integr. Syst.*, vol. 17, no. 9, pp. 1339–1342, 2009. [Online]. Available: <https://doi.org/10.1109/TVLSI.2008.2002046>
- [26] A. L. Fisher and H. T. Kung, "Synchronizing large VLSI processor arrays," *IEEE Trans. Computers*, vol. 34, no. 8, pp. 734–740, 1985. [Online]. Available: <https://doi.org/10.1109/TC.1985.1676619>
- [27] P. Boksberger, F. Kuhn, and R. Wattenhofer, "On the approximation of the minimum maximum stretch tree problem," *Technical report/ETH, Department of Computer Science*, vol. 409, 2003.
- [28] M. James, "Linear solver in linear time." [Online]. Available: <https://www.i-programmer.info/news/181-algorithms/5573-linear-solver-in-linear-time.html>
- [29] R. Fan and N. A. Lynch, "Gradient clock synchronization," *Distributed Comput.*, vol. 18, no. 4, pp. 255–266, 2006. [Online]. Available: <https://doi.org/10.1007/s00446-005-0135-6>
- [30] C. E. Molnar and S. M. Fairbanks, "Control structure for a high-speed asynchronous pipeline," Aug. 10 1999, US Patent 5,937,177.



Matthias Függer received his M.Sc. (2006), and his Ph.D. (2010) in computer engineering from TU Wien, Austria. He worked as an assistant professor at TU Wien and as a post-doctoral researcher at LIX, Ecole Polytechnique, and at MPI for Informatics. Currently, he is a CNRS researcher at LMF, ENS Paris-Saclay, where he leads the Distributed Computing group.



Moti Medina is a faculty member in the engineering faculty at Bar-Ilan University since 2021. Previously he was a faculty member at the School of Electrical & Computer Engineering at the Ben-Gurion University of the Negev since 2017. Previously, he was a post-doc researcher in MPI for Informatics and in the Algorithms and Complexity group at LIAFA (Paris 7). He graduated with his Ph. D., M. Sc., and B. Sc. studies at the School of Electrical Engineering at Tel-Aviv University, in 2014, 2009, and 2007 respectively.

Moti is also a co-author of a text-book on logic design "Digital Logic Design: A Rigorous Approach", Cambridge Univ. Press, 2012.



Johannes Bund is a post-doc researcher at the Faculty of Engineering at Bar-Ilan University since 2022. He graduated with his M. Sc. studies in 2018 at the Saarland Informatics Campus and Max-Planck Institute for Informatics. In 2018 he joined Christoph Lenzen's group at Max-Planck Institute for Informatics as a Ph.D. student. In 2021 he switched, together with Christoph Lenzen, to CISPA Helmholtz Center for Information Security, where he finished his Ph.D. studies.